Published in final edited form as:
Oncogene. 2008 September 18; 27(42): 5599–5611. doi:10.1038/onc.2008.169.

Activation of NF-κB is required for mediating proliferative and anti-apoptotic effects of progastrin on proximal colonic crypts of mice, *in vivo*

Shahid Umar[1,*], **Shubhashish Sarkar**[2,*], **Stephanie Cowey**[2], and **Pomila Singh**[2]

[1]Department of Internal Medicine, University of Texas Medical Branch, Galveston, Texas 77555

[2]Department of Neuroscience and Cell Biology, University of Texas Medical Branch, Galveston, Texas 77555

Abstract

Mice over-expressing progastrin in intestinal mucosa (Fabp-PG mice) are at an increased risk of proximal colon carcinogenesis in response to azoxymethane. In here we report a significant increase in the length of proximal colonic crypts in Fabp-PG mice, associated with potent anti-apoptotic effects of progastrin, which likely contributed to the previously reported increase in colon carcinogenesis in Fabp-PG mice. Phosphorylation of IKKα/β, IκBα and p65NF-κB was significantly elevated in proximal colonic crypts of Fabp-PG versus wild-type mice, which was associated with degradation of IκBα and nuclear translocation/activation of p65. Surprisingly, distal colonic crypt cells were not as responsive to elevated levels of progastrin in Fabp-PG mice. Annexin II, recently described as a high affinity receptor for progastrin, strongly co-localized with progastrin intracellularly and on basolateral membranes of proximal crypt cells, providing evidence that annexin-II binds progastrin *in situ* in colonic crypt cells. Proliferative and anti-apoptotic effects of progastrin on proximal crypts of Fabp-PG mice were attenuated to wild type levels, on treatment with NEMO peptide (an inhibitor of NF-κB activation), demonstrating for the first time a critical role of NF-κB in mediating hyperproliferative affects of progastrin on colonic crypts of Fabp-PG mice, *in vivo*. Thus, down regulation of NF-κB may significantly reduce the increased risk of colon carcinogenesis in response to progastrin.

Keywords

Annexin II; Progastrin; NFκB; ERKs; Fabp-PG mice; NEMO

Introduction

Processing intermediates of gastrin gene products, such as progastrin (PG) exert mitogenic effects *in vitro* and *in vivo* on intestinal mucosal cells (Baldwin et al 2001; Seva et al 1994; Singh et al 2003; Wang et al 1996; Ottewell et al 2003, 2005). Potent anti-apoptotic effects of recombinant human PG (rhPG) were also described on intestinal and pancreatic cancer cells *in vitro* (Wu et al 2003; Rengifo-Cam et al 2007). Transgenic (Tg) mice overexpressing PG from either the liver (hGAS mice) or intestinal epithelial cells (Fabp-PG mice) were at a higher risk for developing pre-neoplastic and neoplastic lesions in colons in response to AOM (Cobb

Correspondence: Pomila Singh, Ph.D., Professor, Department of Neuroscience and Cell Biology, University of Texas Medical Branch, Galveston, Texas 77555-1043, (409) 772-4842, posingh@utmb.edu.
*Both authors contributed equally to this work.

et al 2004; Singh et al 2000a; Singh et al 2000b); treatment with G-Gly (glycine extended gastrin) also increased the risk in rats (Aly et al 2001). Thus, non-amidated gastrins (PG and G-Gly) exert co-carcinogenic effects *in vivo* (Reviewed in Regifo-Cam and Singh 2004).

Under physiological conditions, only processed forms of gastrins (G17, G34) are present in the circulation (as described in Dockray et al 1996). In patients with colorectal cancers and hypergastrinemia (due to various etiologies), elevated levels of circulating PG (0.1 - >1.0 nM) are measured (reviewed in Rengifo-Cam and Singh 2004). Since we reported co-carcinogenic effects of PG in Fabp-PG mice that express 'patho-physiological' concentrations of hPG (< 1 nM – 5 nM) (Cobb et al 2004), it suggests that elevated levels of circulating PG, as measured in certain diseases, may play a role in colon carcinogenesis.

Co-carcinogenic effects of PG could be mediated via either proliferative and/or anti-apoptotic effects on colonic epithelial cells. DNA damaging agents trigger cell death in proliferative zone of colonic crypt cells (Marshman et al 2001). It is possible that mice expressing PG are resistant to apoptotic affect of AOM, which may contribute to the observed increase in colon carcinogenesis in PG expressing mice; this possibility was examined.

We previously reported a significant increase in preneoplastic and neoplastic lesions in proximal versus distal colons of PG expressing mice, in response to AOM (Cobb et al 2004; Singh et al 2000b); mechanisms mediating a differential response remain(s) unknown. One possibility is that proximal colons are more responsive to proliferative and/or anti-apoptotic effects of PG compared to distal colons; this possibility was examined.

Monomeric/heterotetrameric Annexin II, present on extra cellular surface of endothelial and tumor cells, functions as high affinity receptor for plasminogen, tissue plasminogen activator, plasmin (Hajjar et al 1994), and extra cellular matrix protein tenascin-C (Chung and Erickson 1994). Annexin II (ANX-II) is also a high affinity receptor for PG peptides, required for mediating growth effects of PG on intestinal epithelial, colon and pancreatic cancer cells *in vitro* (Rengifo-Cam et al 2007; Singh et al 2007). Differential effects of PG on proximal versus distal colons could be due to differences in interaction of ANX-II with PG in the two parts of colon; this intriguing possibility was examined.

MAP kinases and NF-κB are activated in a pancreatic cancer cell line, *in vitro*, in response to PG (Rengifo-Cam et al 2007). In the current studies we report for the first time a critical role of NFκB activation in mediating proliferative and anti-apoptotic effects of PG on colonic crypt cells *in vivo*. Additionally, our studies provide novel insights into the mechanisms that may be contributing to differential effects of PG on proximal versus distal colonic crypts, which may be clinically relevant in understanding etiology of proximal versus distal colon carcinogenesis in humans.

Results

Length of Colonic Crypts

Crypt lengths in proximal (**P**) colons of Fabp-PG mice were significantly increased compared to that recorded in WT littermates, while crypt lengths in distal (**D**) colons of WT and Fabp-PG mice were similar (Fig1A). Number of cells/crypt column in proximal colons of WT and Fabp-PG mice were ~25 and 55-70 cells, respectively. Length of intact proximal colonic crypts was similarly increased by ~40-50% in Fabp-PG versus WT mice, while length of intact distal colonic crypts was similar in WT versus Fabp-PG mice (Fig1B-C).

Proliferation (PI) and Apoptotic (AI) Indices of Colonic Crypts

Representative sections from proximal colons of WT versus Fabp-PG mice, stained for PCNA, are shown in Fig2A. Based on number of cells labeled/longitudinal crypt, PI was calculated, and data from 50-100 crypts/group of mice are presented in Fig2B. PI was significantly increased in proximal colons of Fabp versus WT mice (Fig2B); PI from distal colons was similar in the two groups of mice (data not shown). A low basal rate of apoptosis (0.2-0.4 cells/crypt) was detected in WT and Fabp-PG mice injected with saline (data not shown), as reported previously (Lishitz et al 2001). Possible protective effects of PG against AOM induced apoptosis was examined. Representative sections from proximal colons of WT and Fabp-PG mice, stained with either H&E (Fig2C), TUNEL assay (Fig2E) or activated-caspase3 antibodies (Fig2G) are shown. Using all three methods, AOM induced apoptosis of proximal colonic crypts was significantly lower in Fabp-PG versus WT mice (Figs2C-H), while AI of distal colonic crypts was similar (data not shown). These results demonstrate the intriguing possibility that PG protects proximal colonic crypts from acute apoptotic effects of AOM on the proliferative zone.

Immunolocalization of PG and its Receptor Annexin-II (ANX-II) in colonic crypts of WT and Fabp-PG mice

Immunostaining for PG was not detected in distal (**D**) or proximal (**P**) colons of WT mice (Fig3). In Fabp-PG mice, the entire longitudinal crypt axis stained positive for PG (Fig3). Relative levels of gastrin cDNA, in distal and proximal colonic crypts of Fabp-PG mice, were similar when measured by quantitative RT-PCR (data not shown). PG was localized to colonic crypts and not detected in interstitial cells (Fig3). Concurrently processed sections in which primary antibody was replaced with purified rabbit IgG, failed to exhibit staining (data not shown). In WT mice, ANX-II staining was localized to baso-lateral and apical membranes of distal and proximal crypts (Fig3). Similarly, in distal crypts of Fabp-PG mice, intense baso-lateral and apical staining for ANX-II was detected (Fig3). However, proximal crypts from Fabp-PG mice exhibited a dramatic increase in cytoplasmic staining with a gradient of increasing crypt base: surface immunoreactivity, similar to that recorded for PG, along with perinuclear staining and some hint of nuclear staining (Fig3). Marked co-localization of ANX-II with PG was observed intracellularly and within the nucleus in proximal colons of Tg mice (Fig3). However, PG and ANX-II co-localized only at baso-lateral, apical and junctional membranes of distal crypts from Fabp-PG mice (Fig3). PG, bound to ANX-II, was differentially retained in distal crypts of Tg mice (Fig3 and Supplementary Fig1A). The *in situ* binding of PG with ANX-II was confirmed by co-immunoprecipitation of PG with ANX-II from proximal and distal crypts of PG mice (Supplementary Fig1B). Relative levels of ANX-II in distal colonic crypts were ~60-80% of that in proximal crypts (Supplementary Fig1B), which may be contributing to the observed loss in retention of PG in distal versus proximal crypts (Fig3, Supplementary Fig1).

Relative levels of phosphorylated ERKs and NF-κB p65 in distal versus proximal colons

Cellular *p*-ERKs (measured by WB analysis of 4-6 separate samples/group), were similar in distal colonic crypts of WT and Fabp-PG mice (data not shown). A significant increase in relative levels of *p*-ERKs was measured in proximal colonic crypts of Fabp-PG versus WT mice (Supplementary Fig2A). Nuclear extracts from distal crypts of Fabp-PG mice were positive for *p*-ERK1/2 (data not shown), but relative levels of nuclear *p*-ERK1/2 were significantly higher in proximal crypts of Fabp-PG versus WT mice (Supplementary Fig2A). The presence of *p*-ERK1/2 in nuclei of proximal crypt cells was confirmed immunohistochemically (Supplementary Fig2B). Cytoplasm, but not nuclei, from distal crypts of both WT and Fabp-PG mice were positive for *p*-ERK (Supplementary Fig2B). However, *p*-ERKs were predominantly present in nuclei of proximal crypts from Fabp-PG mice,

compared to cytoplasmic and occasional nuclear staining in proximal crypts of WT mice (Supplementary Fig2B).

We next examined if NF-κB is activated *in vivo* in Fabp-PG mice via the canonical pathway. Data from Western blots (n=5 mice/group) were densitometrically analyzed for each molecule, and presented as a ratio of *p*-IKKα/β:IKKα/β in Fig4A. Relative levels of total IKKs were similar in cellular extracts from proximal and distal crypts of WT mice, and assigned a 100% value (Fig4A). Ratio of phosphorylated versus total IKKα/β was many-fold higher in proximal crypts of Fabp-PG mice compared to all other groups (Fig4A).

Representative WB from 1/5 mouse samples, for phosphorylated and total IκBα are presented in Fig4B; ratio of phosphorylated versus total IκBα from all samples are shown as bar graphs in Fig4C. Relative levels of *p*-IκBα increased significantly in proximal versus distal crypts of Fabp-PG mice, while *p*-IκBα levels in distal and proximal colons of WT mice were similar. WB data were confirmed immunohistochemically, wherein the accumulation of *p*-IκBα was increased in proximal but not distal crypts of Fabp-PG mice; the difference was less dramatic in proximal versus distal crypts of WT mice (Fig4D). Negative controls stained with non-immune IgG are presented in Supplementary Fig3A. Crypts from all groups were positive for basal levels of *p*-IκBα in cytosol and nuclei. A significant increase in *p*-IκBα in proximal crypts of Fabp-PG mice was associated with degradation of IκBα (Fig4B-**lower panel**)

Degradation of IκBα results in translocation of NF-κB to nuclei. Representative WB data from 1/5 mouse samples, demonstrating *p*-p65 and total p65 levels are presented in Fig5A. NFκBp65 levels were similar in distal and proximal crypts of WT mice; baseline levels of total p65 were elevated in distal and proximal crypts of Tg mice (Fig5A), suggesting possible increase in expression/stabilization of p65 in Tg versus WT mice. Transcriptional activity of NF-κB is controlled by phosphorylation at Serines 276, 529 and 536 (Hayden and Ghosh 2004). We found that relative levels of pp65^{276}, but not pp65^{536}, increased in cellular (Fig5A) and nuclear (Fig5B) extracts of proximal crypts from Tg versus WT mice by >five-fold; no significant differences were measured in distal crypts of WT and Tg mice (Figs5A-B). To confirm activation of p65, DNA binding assays were conducted using Active Motif kit, as previously described (Rengifo-Cam et al 2007). A significant increase in DNA binding of nuclear extracts from proximal versus distal crypts of Tg mice were measured (Fig5C); no significant differences were measured in distal and proximal crypts of WT mice (Fig5C). Presence of both p50 and p65 was confirmed in DNA binding assay using specific antibodies, suggesting that p50/p65 heterodimers are translocated to nucleus in proximal colons of Tg mice (data not shown). IHC revealed presence of basal staining for pp65^{276} in cytosol and nuclei of crypts from all groups (Fig5D). However, significant increases in both cytoplasmic and nuclear staining for pp65^{276} was observed in proximal colons of Fabp-PG mice compared to all other groups (Fig5Di); enlarged images of proximal and distal crypts from Tg mice are shown as Supplementary Fig4. Cells positive for nuclear staining for *p*-p65^{276}/crypt were counted; data in Fig5Dii confirms WB data. Concurrently processed crypts in which primary antibody was replaced with purified mouse IgG, failed to exhibit staining (Supplementary Fig3B). IHC with antibodies specific for *p*-p65^{536} exhibited weak immunoreactivity in both proximal and distal sections of Fabp-PG and WT mice (data not shown), correlating with biochemical data in Fig5A-B. These findings suggest that NF-κB activation in proximal colons of Fabp-PG mice involves degradation of IκBα, followed by phosphorylation and activation of p65, which likely provides survival advantages to proliferating colonocytes in proximal colons of Fabp-PG mice thus resulting in observed differences in length of proximal crypts from Fabp-PG versus WT micem shown in Fig1.

Activation of NF-κB is required for mediating proliferative and anti-apoptotic effects of PG on proximal crypts

Fabp-PG mice were treated with either NEMO peptide, an inhibitor of IKKα/β, or control peptide. Treatment of Fabp-PG mice with NEMO did not result in loss of ERK phosphorylation (Fig6A), but significantly inhibited phosphorylation of IKKα/β at Ser176/180 (Fig6B) and IκBα at Ser32/36 (Fig6C); this confirmed specific effect of NEMO on IKK signaling pathway. Loss of IκBα phosphorylation in proximal crypts (Fig6C), resulted in inhibition of NFκB activity in a DNA binding assay in samples from NEMO versus control peptide treated mice (Fig6Di); basal level of activation measured in NEMO treated samples of proximal crypts was similar to that measured in corresponding control and NEMO treated distal crypts (upper and lower panels of Fig6Di).

Loss in NFκB activation, correlated with a loss in relative levels of *p*-p65^{276} in nuclei of proximal crypts, measured biochemically (Fig6Dii) and by IHC (Fig6Diii). NFκB inhibition *in vivo* was associated with a significant loss in number of BrdU positive cells in proximal crypts of NEMO-treated Fabp-PG mice (Fig6Ei), leading to decrease in PI of proximal colons (Fig6Eii), compared to that in control peptide treated samples. This led to a significant loss in anti-apoptotic effects of PG on proximal crypt cells, as evidenced by a 2-3 fold increase in relative levels of activated-caspase3 in NEMO versus control peptide treated samples (Fig6F). These results suggest, for the first time, a critical role for NF-κB in mediating proliferative and anti-apoptotic effects of PG on proximal colonic crypts *in vivo*. Relative levels of activated NFκB in proximal colons of NEMO treated Fabp-PG mice were reverted to levels measured in proximal colons of WT mice (Fig5C).

Discussion

We previously reported significant increase in proximal colon carcinogenesis in transgenic (Tg) mice over-expressing PG, in response to AOM (Cobb et al 2004; Singh et al 2000a, Singh et al 2000b). Our current results suggest that both an increase in proliferation and decrease in AOM induced apoptosis may contribute to the increase in proximal colon carcinogenesis in Tg mice. An increase in crypt cell proliferation from distal to proximal colons has been noted in normal human colons and in patients positive for sporadic colon cancers (Mills et al 2001); it remains to be seen if the reported difference in humans are perhaps due to differential effects of growth factors (such as PG).

Mechanism(s) mediating differences in cancer cell biology of proximal versus distal colons are unknown. Proximal and distal colons are embryonically derived from mid-gut and hind-gut, respectively (Johnson and McCormack 1994). Stem cells are located at the base in distal colons and towards the middle in proximal colons (Sato and Ahnen 1992). Proximal and distal colorectal carcinomas (CRCs) exhibit differences in incidence in relation to geographic region, age, gender, and hereditary cancer syndromes, suggesting two categories of CRC based on site and origin in the colon (Iacopetta 2002). Differences in expression of adenosine receptor subtypes, and response to adenosine, were reported in proximal versus distal colons of mice (Zizzo et al 2006). Methylation mediated silencing of mismatched repaired genes are significantly higher in proximal versus distal sporadic microsatellite instability CRCs (Watanabe et al 2006). Significant differences in expression of Bak (Liu et al 1999) and cErbB2 (Fric et al 2000), are present in right and left colons. Significant differences were reported in gene expression profiles of right versus left colons during embryonic development, which were amplified during post natal development, which may explain differences in susceptibility of proximal versus distal colons to specific pathways of tumorigenesis (Glebov et al 2003). Thus differences in origin, biology and genetic expression profiles, may have contributed to the observed differences in proliferative and survival effects of PG on proximal versus distal colons of Fabp-PG mice.

We recently reported activation of NFκB in pancreatic cancer cells in response to PG *in vitro* (Rengifo-Cam et al 2007). Our current studies demonstrate for the first time, that NFκB is activated differentially in proximal versus distal colons of Fabp-PG mice. Our studies demonstrate that PG up-regulates phosphorylation of IKKα/β, resulting in degradation of IκBα and nuclear translocation/activation of phosphorylated NF-κBp65 in proximal, but not distal, crypts of Tg mice; differences in activation of NF-κB pathway, may contribute to differences in PI and length of proximal versus distal crypts in Tg mice.

Multiple signaling pathways lead to phosphorylation and activation of IKK complexes (Hayden and Ghosh 2004). MAPKs/ERKs were required for activating NF-κB in response to PG, *in vitro* (Rengifo-Cam et al, 2007). In the current study, we measured a significant increase in phosphorylation/activation of ERKs in proximal, but not distal, crypts of Tg mice, which may explain significant difference in activation of NF-κB in proximal versus distal crypts of Tg mice. Perhaps the most important finding was that NF-κB activation was required for mediating proliferative/anti-apoptotic effects of PG on proximal crypt cells (Fig6).

Several receptor subtypes mediate biological effects of gastrin/progastrin peptides (reviewed in Rengifo-Cam and Singh 2004). Growth factor effects of PG and G-Gly peptides are mediated by novel receptor mechanisms, distinct from CCK_2R and CCK_1R (Seva et al 1994; Rengifo-Cam et al 2004; Ahmed et al 2005). Earlier, we had identified a 33-36 kDa protein as a high affinity binding protein for progastrin/gastrin peptides, which was pharmacologically different from CCK_1R and CCK_2R (Chicone et al 1989). Recently we discovered that ANX-II represented the novel p36 receptor protein (Singh et al 2007). Unlike CCK_2R-Abs, ANX-II-Abs completely attenuated growth effects of PG on AR42J cells and IEC cells *in vitro* (Rengifo-Cam et al 2007; Singh et al 2007), and ANX-II expression was required for measuring growth effects of autocrine PG in a human colon cancer cell line (Singh et al 2007). Studies to-date have reported only growth promoting and anti-apoptotic effects of non-amidated gastrins (reviewed in Rengifo-Cam and Singh 2004). G17, either stimulates (Song et al 2003) or inhibits (Műerkőster et al 2007) growth of target cells via CCK_2R, which may reflect relative expression of CCK_2R versus Annexin II on target cells, as recently reviewed (Singh 2007).

In the current studies we report for the first time *in situ* co-localization of ANX-II with PG in colonic crypts of Fabp-PG mice. A novel and surprising finding was that co-localization of ANX-II with PG was significantly different in proximal versus distal crypts of Fabp-PG mice. While ANX-II strongly co-localized with PG intracellularly in proximal crypts, in distal crypts, ANX-II co-localized with PG only near baso-lateral and apical membranes of Fabp-PG mice. As expected, PG was not detected in crypts of WT mice, and ANX-II was largely present along baso-lateral and apical membranes of both proximal and distal crypts of WT mice, similar to the pattern observed in distal crypts of Fabp-PG mice. These results suggest the novel possibility that in the presence of PG, ANX-II becomes internalized in proximal, but not distal, crypts of PG mice. In preliminary studies, we have similarly reported intracellular co-localization of PG with ANX-II in intestinal epithelial cells in response to PG (Sarkar et al 2007).

Based on our studies so far, it appears that ANX-II is required for mediating biological effects of PG on target cells. Similarly, tissue plasminogen activator (tPA) which functions as a protease and a cytokine, strongly co-localized with EGFR and ANX-II in pancreatic cancer cells (Ortiz-Zapater et al 2007), and the authors concluded that tPA enhances growth of pancreatic cancer cells via interacting with EGFR and ANX-II. Binding of ligands with ANX-II results in activation of several signaling pathways including NF-κB, JAK/STAT, p38 MAPK, MEKK4 (MAPK/ERK kinase kinase) (reviewed in Singh 2007). It is possible that internalization and co-localization of ANX-II with PG in proximal but not distal colonic crypts of Fabp-PG mice, provides the required platform for activation of several kinases resulting in

the observed activation of Src, PI3K/Akt, JAK 2, STAT 5/3, ERKs, p38 MAPK and NF-κB, in response to PG in various target cells (Rengifo-Cam et al 2007; Ferrand et al 2005), as diagrammatically presented in a review article (Singh 2007).

In summary, we demonstrate for the first time that PG significantly reduces apoptotic effects of AOM, *in vivo*, on the proliferative zone of proximal colonic crypt cells. The dual effect of increasing proliferation and decreasing AOM induced apoptosis, may have resulted in the previously reported increase in proximal colon carcinogenesis in response to AOM in Fabp-PG mice (Cobb et al 2004). Additionally, in the current studies we demonstrate for the first time that NF-κB is activated *in vivo* in response to PG in proximal colonic crypt cells of Fabp-PG mice, and that activation of NF-κB is critically required for mediating proliferative and anti-apoptotic effects of PG on proximal crypt cells. Significant differences in intracellular localization of Annexin II, bound to PG, in proximal versus distal colonic crypts may provide the underlying mechanism for the differential activation of growth promoting/anti-apoptotic signaling pathways, resulting in the observed differences in length of proximal versus distal colonic crypts in transgenic mice. Innate differences in biology of proximal versus distal colonic crypts, resulting in differential retention of PG, bound to ANX-II, in proximal vs distal crypts, may be an additional contributing factor, which needs to be further examined.

Materials and Methods

Housing of Fabp-PG mice

Fabp-PG mice were generated as described (Cobb et al 2004). Fatty acid binding protein (Fabp) promoter was used to drive expression of human gastrin cDNA in small and large intestines. Fabp-PG mice and their WT littermates were bred and housed in animal housing facility at UTMB, using protocols approved by Institutional Animal Care and Use Committee at UTMB, as described (Cobb et al 2004). Only homozygous Fabp-PG mice (Tg/Tg) were used and confirmed by semi-quantitative cycle PCR as described (Cobb et al 2004). Fabp-PG mice were positive for 0.5-2.0 nM PG in the plasma while WT mice were negative (Cobb et al 2004). Circulating levels of amidated gastrins (G17) were similar in Fabp-PG and WT mice (~30 pM).

Treatment of Mice with NEMO Peptide

Peptides corresponding to NEMO-binding domain (NBD) of IKKα or IKKβ specifically inhibit the induction of NFκB activation without inhibiting basal NFκB activity (May et al 2000). Therefore, to understand role of induced activation of NFκB in mediating proliferative/anti-apoptotic effects of PG in Fabp-PG mice, we treated mice with either wtNBD (NEMO peptide) or a control peptide (Imgenex, San Diego, CA), as described (Dasgupta et al 2004). Peptides were solubilized in saline and mice injected ip with 1.25mg/kg body weight, once daily for 4 days. The last injection was given 2h before sacrifice.

Isolation of Colonic Crypts

Intact colonic crypts were isolated from mice, as described previously (Umar et al 2003). Crypts were imaged on an inverted microscope with a 12-bit gray level charge-coupled device camera. Images were taken at 200× magnification and crypt length measured, using a standard microscale etched onto a glass slide using Metamorph image analysis software (Universal Imaging Corp., Brandywine Parkway, PA). A total of ~150 crypts/group were used for length measurements.

PCNA and BrdU staining of colonic crypts as a measure of Proliferative Index (PI)

Proliferating cells were identified immunohistochemically by staining colonic sections for proliferating cell nuclear antigen (PCNA), as described previously (Umar et al 2000). The % of dark stained cells per longitudinally oriented crypt was calculated as the PI. Ten well-oriented crypts were counted distally and proximally per animal. In a few experiments, mice were injected intraperitoneally with 5′-bromo-deoxyuridine (BrdU; Roche Diagnostics, Germany) (160 mg/kg body wt) 2h before death to label S-phase cells. Frozen sections from proximal and distal colons were processed for BrdU staining as described previously (Singh et al 2000b).

Histological and Immunocytochemical (IHC) Analysis of Colonic Crypts for Measuring Markers of Apoptotic Death

Azoxymethane (AOM; Sigma-Aldrich, St. Louis, MO) induces G to A point mutations in colonic cells, resulting in apoptosis (Hong et al 1999). Mice were injected intraperitoneally with AOM (20mg/Kg body weight) (Singh et al 2000b) and sacrificed after 24h. Colons were collected and fixed flat on Whatman filter paper in 10% formalin as described (Cobb et al 2004; Singh et al 2000b), and processed by standard histological techniques. Sections (4μm) stained with hematoxylin and eosin (H&E) were scored for apoptotic bodies. A duplicate set of colonic sections were subjected to terminal transferase mediated dUTP-biotin nick end labeling (TUNEL) staining using in situ cell death detection kit (Roche Diagnostics). Total number of apoptotic cells within 10 well-oriented longitudinal crypts from distal and proximal colons of each mouse were counted (5 mice/group). Apoptotic index (AI) was calculated as % apoptotic cells/crypt.

Caspases are activated in colonic crypt cells in proliferative zone in response to 1,2-dimethylhydrazine (Lifshitz et al 2001). We processed colonic sections for IHC with anti-active caspase-3 antibody. Slides were deparaffinized and incubated in methanol with 3% H_2O_2 for 15 min, and rinsed with PBS. Horse blocking serum was added for 20 minutes, and slides incubated overnight with anti-caspase-3 antibody at 1:400 dilution (R&D Systems, Minneapolis, MN), and with biotinylated secondary anti-rabbit antibody (1:200 dilution), followed by avidin-peroxidase reagent (Vectastain Elite ABC kit, Vector Laboratories In., Burlingame, CA), and DAB. Control slides were treated with non-immune IgG. Slides were viewed at 40× magnification with bright field microscopy, and number of stained cells within the crypts per field of view (usually about 7 crypts), were recorded. Fifteen fields of view were examined for each mouse sample (5 mice/group).

Western Immunoblot (WB) Analysis

Intact colonic crypts pelleted from proximal/distal colons were homogenized in lysis buffer, and cellular and nuclear extracts prepared as described previously (Rengifo-Cam et al 2007; Wang et al 2006). Protein concentrations were determined, and extracts frozen at -70°C. lysates were processed for WB with the indicated antibodies as described previously (Rengifo-Cam et al 2007; Umar et al 2007).

Primary antibodies used for WB, included: polyclonal anti-ERK1/2 (p44/42), ERK1/2-Thr^{202}/Tyr^{204} (*p*-p44/42), IKKα/β, IKKα/β-Ser$^{176/180}$, IκBα, IκBα-Ser$^{32/36}$, p65, p65-Ser^{276}, p65-Ser^{536} (Cell Signaling Technology, Beverly, MA); polyclonal anti-Annexin-II, laminB (Santa Cruz Biotechnology, Santa Cruz, CA); monoclonal anti-Caspase-3 (Pharmingen); and monoclonal anti-β-actin (Chemicon International, Temecula, CA). Mono-specific polyclonal anti-PG-antibody was generated by using an rhPG-affinity column, in the Core Facility at UTMB, and used as described previously (Cobb et al 2004). Primary antibodies bound to protein bands on WB membranes were detected with horseradish peroxidase-conjugated anti-

mouse or anti-rabbit secondary antibodies, and developed using ECL detection system (Amersham Corp., Arlington Heights, IL, USA).

Immunohistochemical Detection of Signaling Molecules

Immunohistochemistry (IHC) for phospho ERKs, IKKα/β, IκBα, p65 NF-κB was performed on 5-μm-thick frozen sections utilizing HRP labeled polymer conjugated to secondary antibody using Envision+ System-HRP (DAB; Dako Cytomation, Carpinteria, CA) with microwave accentuation as described previously (Wang et al 2006). Nuclei were stained with hematoxylin.

For immunofluorescence (IMF) detection of PG and ANX-II

For immunofluorescence (IMF) detection of PG and ANX-II, sections were deparaffinized and subjected to antigen retrieval as described (Wang et al 2006). Sections were incubated O/N at 4°C with anti-PG and anti-ANX-II antibodies, followed by incubation with secondary antibodies conjugated to Texas Red and FITC, respectively. Slides were washed and incubated with DAPI for 5 min at RT to stain nuclei, and mounted on alcohol-cleaned slides in anti-fade media [1% phenylenediamine antioxidant in PBS (pH 9.0) in 90% glycerol] and analyzed via fluorescent microscopy, using Axiophot 2 microscope (Carl Zeiss, Germany). Controls included either omission of primary antibody or detection of endogenous IgG staining pattern with goat anti-mouse or anti-rabbit IgG (Calbiochem, San Diego, CA).

Statistical Analysis

Data are presented as the mean ± SEM of values obtained from 3-5 mouse samples/experiment × 2. To test for significant differences between means, nonparametric Mann-Whitney test was employed using Statview 4.1 (Abacus Concepts, Inc., Berkeley, CA); P values were considered to be statistically significant if less than 0.05.

Supplementary Material

Refer to Web version on PubMed Central for supplementary material.

Acknowledgments

This work was supported by grant #s CA97959 and CA114264 to P. Singh, and Grant # CA099121 to S. Umar from the NIH.

References

Ahmed S, Murphy RF, Lovas S. Importance of N- and C-terminal regions of gastrin-Gly for preferential binding to high and low affinity gastrin-Gly receptors. Peptides 2005;26:1207–1212. [PubMed: 15949639]

Aly A, Shulkes A, Baldwin GS. Short term infusion of glycine-extended gastrin(17) stimulates both proliferation and formation of aberrant crypt foci in rat colonic mucosa. Int J Cancer 2001;94:307–313. [PubMed: 11745407]

Baldwin GS, Hollande F, Yang Z, Karelina Y, Paterson A, Strang R, Fourmy D, Neumann G, Shulkes A. Biologically active recombinant human progastrin(6-80) contains a tightly bound calcium ion. J Biol Chem 2001;276:7791–7796. [PubMed: 11113148]

Chicone L, Narayan S, Townsend CM Jr, Singh P. The presence of a 33-40 KDa gastrin binding protein on human and mouse colon cancer. Biochem Biophys Res Commun 1989;164:512–519. [PubMed: 2803316]

Chung CY, Erickson HP. Cell surface Annexin II is a high affinity receptor for the alternatively spliced segment of tenascin-C. J Cell Biol 1994;126:539–548. [PubMed: 7518469]

Cobb S, Wood T, Ceci J, Varro A, Velasco M, Singh P. Intestinal expression of prograstin significantly increases colon carcinogenesis in transgenic mice in response to AOM. Cancer 2004;100:1311–1323. [PubMed: 15022301]

Dasgupta S, Jana M, Zhou Y, Fung YK, Ghosh S, Pahan K. Antineuroinflammatory effect of NF-kappaB essential modifier-binding domain peptides in the adoptive transfer model of experimental allergic encephalomyelitis. J Immunol 2004;173:1344–1354. [PubMed: 15240729]

Dockray GJ, Varro A, Dimaline R. Gastric endocrine cells: gene expression, processing, and targeting of active products. Physiol Rev 1996;76:767–798. [PubMed: 8757788]

Ferrand A, Bertrand C, Portolan G, Cui G, Carlson J, Pradayrol L. Signaling pathways associated with colonic mucosa hyperproliferation in mice overexpressing gastrin precursors. Cancer Res 2005;65:2770–2777. [PubMed: 15805277]

Fric P, Sovova V, Sloncova E, Lojda Z, Jirasek A, Cermak J. Different expression of some molecular markers in sporadic cancer of the left and right colon. European Journal of Cancer Prevention 2000;9:265–268. [PubMed: 10958329]

Glebov OK, Rodriguez LM, Nakahara K, Jenkins J, Cliatt J, Humbyrd CJ. Distinguishing right from left colon by the pattern of gene expression. Cancer Epidemiol Biomarkers Prev 2003;12:755–762. [PubMed: 12917207]

Hajjar KA, Jacovina AT, Chacko J. An endothelial cell receptor for plasminogen/tissue plasminogen activator. I. Identity with Annexin II. J Biol chem 1994;269:21191–21197. [PubMed: 8063740]

Hayden MS, Ghosh S. Signaling to NF-kappa B. Genes & Development 2004;18:2195–2224. [PubMed: 15371334]

Hong MY, Chapkin RS, Wild CP, Morris JS, Wang N, Carroll RJ, Turner ND, Lupton JR. Relationship between DNA adduct levels, repair enzyme, and apoptosis as a function of DNA methylation by azoxymethane. Cell Growth Differ 1999;10:749–758. [PubMed: 10593651]

Iacopetta B. Are there two sides to colorectal cancer? Int J Cancer 2002;101:403–408. [PubMed: 12216066]

Johnson, LR.; McCormack, SA. Physiology of the Gastrointestinal Tract. 3rd. New York: Raven Press; 1994.

Lifshitz S, Lamprecht SA, Benharroch D, Prinsloo I, Polak-Charcon S, Schwartz B. Apoptosis (programmed cell death) in colonic cells: from normal to transformed stage. Cancer Lett 2001;163:229–238. [PubMed: 11165759]

Liu LU, Holt PR, Krivosheyev V, Moss SF. Human right and left colon differ in epithelial cell apoptosis and in expression of Bak, a pro-apoptotic Bcl-2 homologue. Gut 1999;45:45–50. [PubMed: 10369703]

Marshman E, Ottewell PD, Potten CS, Watson AJ. Caspase activation during spontaneous and radiation-induced apoptosis in the murine intestine. J Pathol 2001;195:285–292. [PubMed: 11673824]

May MJ, D'Acquisto F, Madge LA, Glöckner J, Pober JS, Ghosh S. Selective inhibition of NF-kappaB activation by a peptide that blocks the interaction of NEMO with the IkappaB kinase complex. Science 2000;289:1550–1554. [PubMed: 10968790]

Mills SJ, Mathers JC, Chapman PD, Burn J, Gunn A. Colonic crypt cell proliferation state assessed by whole crypt microdissection in sporadic neoplasia and familial adenomatous polyposis. Gut 2001;48:41–46. [PubMed: 11115821]

Müerköster S, Isberner A, Arlt A, Witt M, Reimann B, Blaszczuk E, Werbing V, Fölsch UR, Schmitz F, Schäfer H. Gastrin suppresses growth of CCK2 receptor expressing colon cancer cells by inducing apoptosis in vitro and in vivo. Gastroenterology 2005;129:952–968. [PubMed: 16143134]

Ortiz-Zapater E, Peiró S, Roda O, Corominas JM, Aguilar S, Ampurdanés C, Real FX, Navarro P. Tissue plasminogen activator induces pancreatic cancer cell proliferation by a non-catalytic mechanism that requires extracellular signal-regulated kinase 1/2 activation through epidermal growth factor receptor and annexin A2. American Journal of Pathology 2007;170:1573–1584. [PubMed: 17456763]

Ottewell PD, Watson AJ, Wang TC, Varro A, Dockray GJ, Pritchard DM. Progastrin stimulates murine colonic epithelial mitosis after DNA damage. Gastroenterology 2003;124(5):1348–57. [PubMed: 12730875]

Ottewell PD, Varro A, Dockray GJ, Kirton CM, Watson AJ, Wang TC, Dimaline R, Pritchard DM. COOH-terminal 26-amino acid residues of progastrin are sufficient for stimulation of mitosis in murine colonic epithelium *in vivo*. Am J Phsyiol Gastrointest Liver Physiol 2005;288(3):G541–9.

Rengifo-Cam W, Singh P. Role of progastrins and gastrins and their receptors in GI and pancreatic cancers: targets for treatment. Curr Pharm Des 2004;10:2345–2358. [PubMed: 15279613]

Rengifo-Cam W, Umar S, Sarkar S, Singh P. Anti-apoptotic effects of progastrin on pancreatic cancer cells are mediated by sustained activation of nuclear factor κB. Cancer Res 2007;67:7266–7274. [PubMed: 17671195]

Sarkar S, Umar S, Singh G, Singh P. Progastrin (PG) peptide co-localizes with Annexin II (ANX-II), in situ, in human colon cancer cells (HCT-116), expressing autocrine PG, and in intestinal epithelial cells (IEC-18) in response to PG stimulation. Gastroenterology 2007;132:A540–A541.

Sato M, Ahnen DJ. Regional variability of colonocyte growth and differentiation in the rat. Anat Rec 1992;233:409–414. [PubMed: 1376970]

Seva C, Dickinson CJ, Yamada T. Growth-promoting effects of glycine-extended progastrin. Science 1994;265:410–412. [PubMed: 8023165]

Singh P, Velasco M, Given R, Varro A, Wang TC. Progastrin expression predisposes mice to colon carcinomas and adenomas in response to a chemical carcinogen. Gastroenterology 2000A;119:162–171. [PubMed: 10889165]

Singh P, Velasco M, Given R, Wargovich M, Varro A, Wang TC. Mice overexpressing progastrin are predisposed for developing aberrant colonic crypt foci in response to AOM. American Journal of Physiology-Gastrointestinal and Liver Physiology 2000B;278:G390–G399. [PubMed: 10712258]

Singh P, Lu X, Cobb S, Miller BT, Tarasova N, Varro A, Owlia A. Progastrin1-80 stimulates growth of intestinal epithelial cells in vitro via high-affinity binding sites. Am J Physiol Gastrointest Liver Physiol 2003;284:G328–G339. [PubMed: 12388191]

Singh P, Wu H, Clark C, Owlia A. Annexin II binds progastrin and gastrin-like peptides, and mediates growth factor effects of autocrine and exogenous gastrins on colon cancer and intestinal epithelial cells. Oncogene 2007;26:425–440. [PubMed: 16832341]

Singh P. Role of Annexin-II in GI cancers: Interaction with gastrins/progastrins. Cancer Lett 2007;252:19–35. [PubMed: 17188424]

Song DH, Rana B, Wolfe JR, Crimmins G, Choi C, Albanese C. Gastrin-induced gastric adenocarcinoma growth is mediated through cyclin D1. Am J Physiol Gastrointest Liver Physiol 2003;285:G217–G222. [PubMed: 12606305]

Umar S, Sellin JH, Morris AP. Increased nuclear translocation of catalytically active PKC-zeta during mouse colonocyte hyperproliferation. Am J Physiol Gastrointest Liver Physiol 2000;279:G223–G237. [PubMed: 10898766]

Umar S, Morris AP, Kourouma F, Sellin JH. Dietary pectin and calcium inhibit colonic proliferation in vivo by differing mechanisms. Cell Prolif 2003;36:361–375. [PubMed: 14710853]

Umar S, Wang Y, Morris AP, Sellin JH. Dual alterations in casein kinase I-epsilon and GSK-3beta modulate beta-catenin stability in hyperproliferating colonic epithelia. Am J Physiol Gastrointest Liver Physiol 2007;292:G599–G5607. [PubMed: 17053159]

Wang TC, Koh TJ, Varro A, Cahill RJ, Dangler CA, Fox JG, Dockray GJ. Processing and proliferative effects of human progastrin in transgenic mice. J Clin Invest 1996;98:1918–1929. [PubMed: 8878444]

Wang Y, Xiang GS, Kourouma F, Umar S. Citrobacter rodentium-induced NF-kappa B activation in hyperproliferating colonic epithelia: role of p65 (Ser(536)) phosphorylation. British Journal of Pharmacology 2006;148:814–824. [PubMed: 16751795]

Watanabe T, Kobunai T, Toda E, Yamamoto Y, Kanazawa T, Kazama Y. Distal colorectal cancers with microsatellite instability (MSI) display distinct gene expression profiles that are different from proximal MSI cancers. Cancer Res 2006;66:9804–9808. [PubMed: 17047040]

Wu H, Owlia A, Singh P. Precursor peptide progastrin(1-80) reduces apoptosis of intestinal epithelial cells and upregulates cytochrome c oxidase Vb levels and synthesis of ATP. Am J Physiol Gastrointest Liver Physiol 2003;285:G1097–G1110. [PubMed: 12881229]

Zizzo MG, Mule F, Serio R. Inhibitory responses to exogenous adenosine in murine proximal and distal colon. British Journal of Pharmacology 2006;148:956–963. [PubMed: 16847444]

Abbreviations

ANX-II	Annexin-II
IκB	Inhibitor of kappa B
IKK	IκB Kinase
NF-κB	Nuclear Factor-kappa B
PG	Progastrin
WT	wild type littermates
Tg	transgenic
WB	Western blot

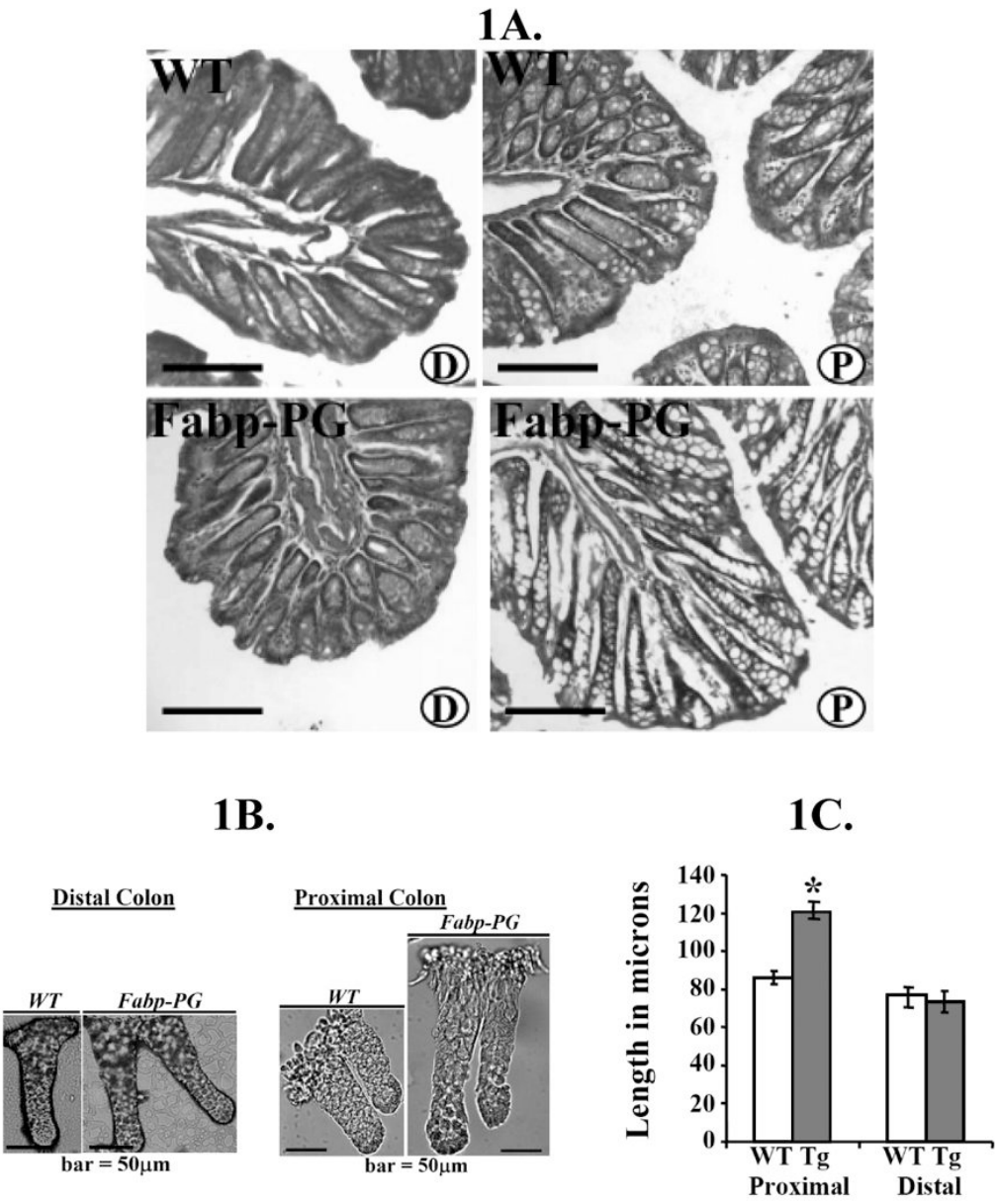

Figure 1.

A. H&E stain of formalin-fixed cryosections (5μm) from distal (D) and proximal (P) colons of WT and Fabp-PG mice (magnification, ×4). (n = 10 mice/group; scale bar = 150 μm). **B.** Representative images of the intact distal and proximal colonic crypts from WT and Fabp-PG mice (n = 10 mice/group; scale bar = 50μm). **C.** The length of intact colonic crypts isolated from both WT and Fabp-PG mice were measured using Metamorph image analysis software as described in Methods and the results from 150 crypts/group of mice are shown in **C.** * = P <0.05 versus WT as measured by students' t-test.

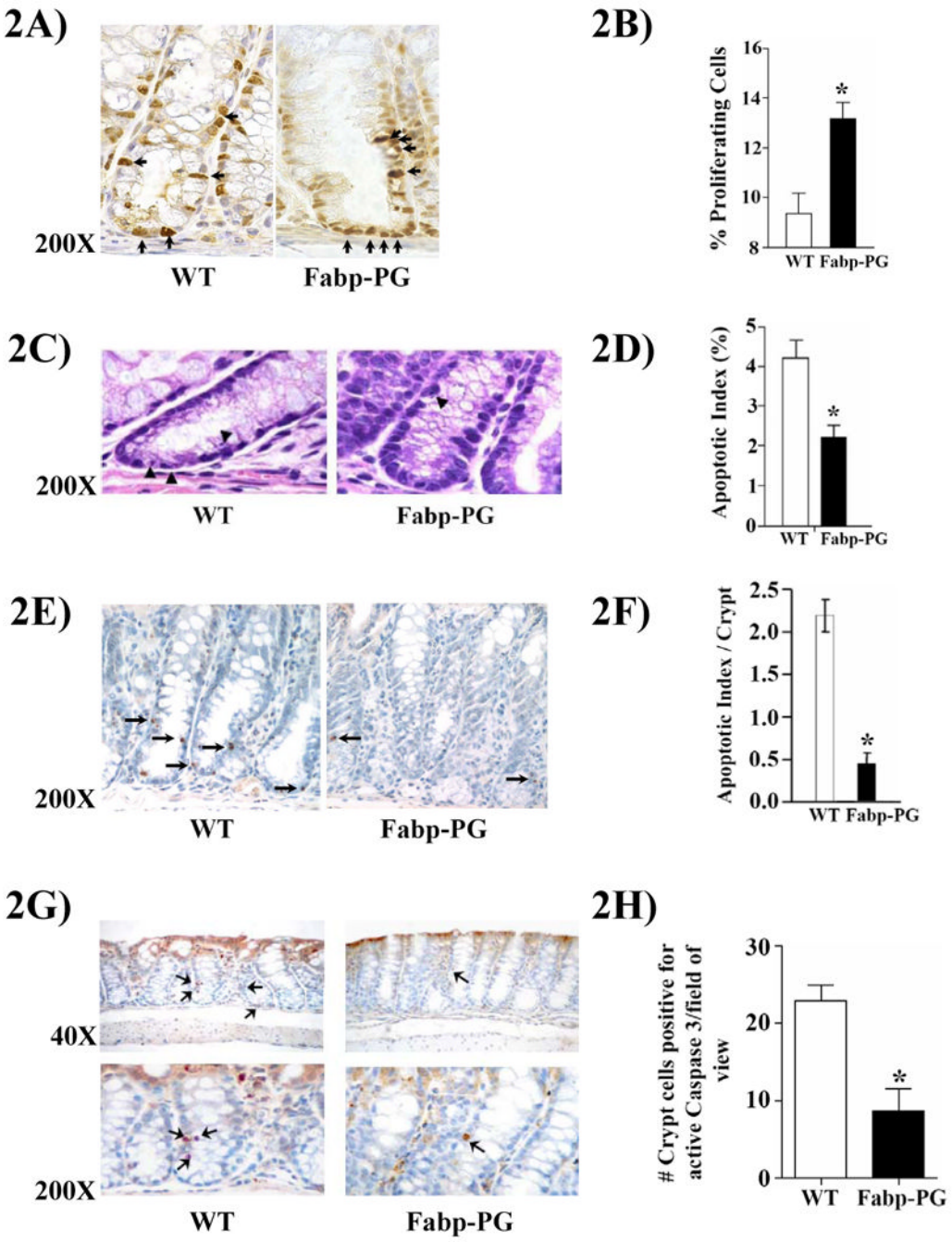

Figure 2.

A-B. Proliferative index. Representative sections from Fabp-PG versus WT, stained with proliferating cell nuclear antigen antibody **(A)**. PI was calculated based on number of positive cells along the longitudinal crypt axis **(B)**. Data in **B** were derived from 55-102 crypts/5-10 mice/group. **C-F. Apoptotic** Index. Representative H&E stained sections from proximal colons of AOM-treated WT and Fabp-PG mice are shown in **C**. Arrowheads identify apoptotic bodies, and data from 76-224 crypts/group of mice (5-10 mice/group) are shown in **D** as mean ± SEM. TUNEL staining of representative longitudinal sections of colonic crypts from proximal colon is shown in **E**; arrows point to positively stained (apoptotic) cells and data from 48-98 crypts/group of mice is presented in **F** as mean ± SEM. **G-H. IHC for activated caspase**

3. Representative longitudinal sections of proximal colons, immunostained for activated caspase 3, are shown in **G** at 40× and 200 × magnifications. Arrows point to positively stained cells. Number of apoptotic cells/75 fields of view from proximal colons of 5 mice in a group are shown as mean ± SEM in **H**. * = $P<0.05$ versus WT values in each case.

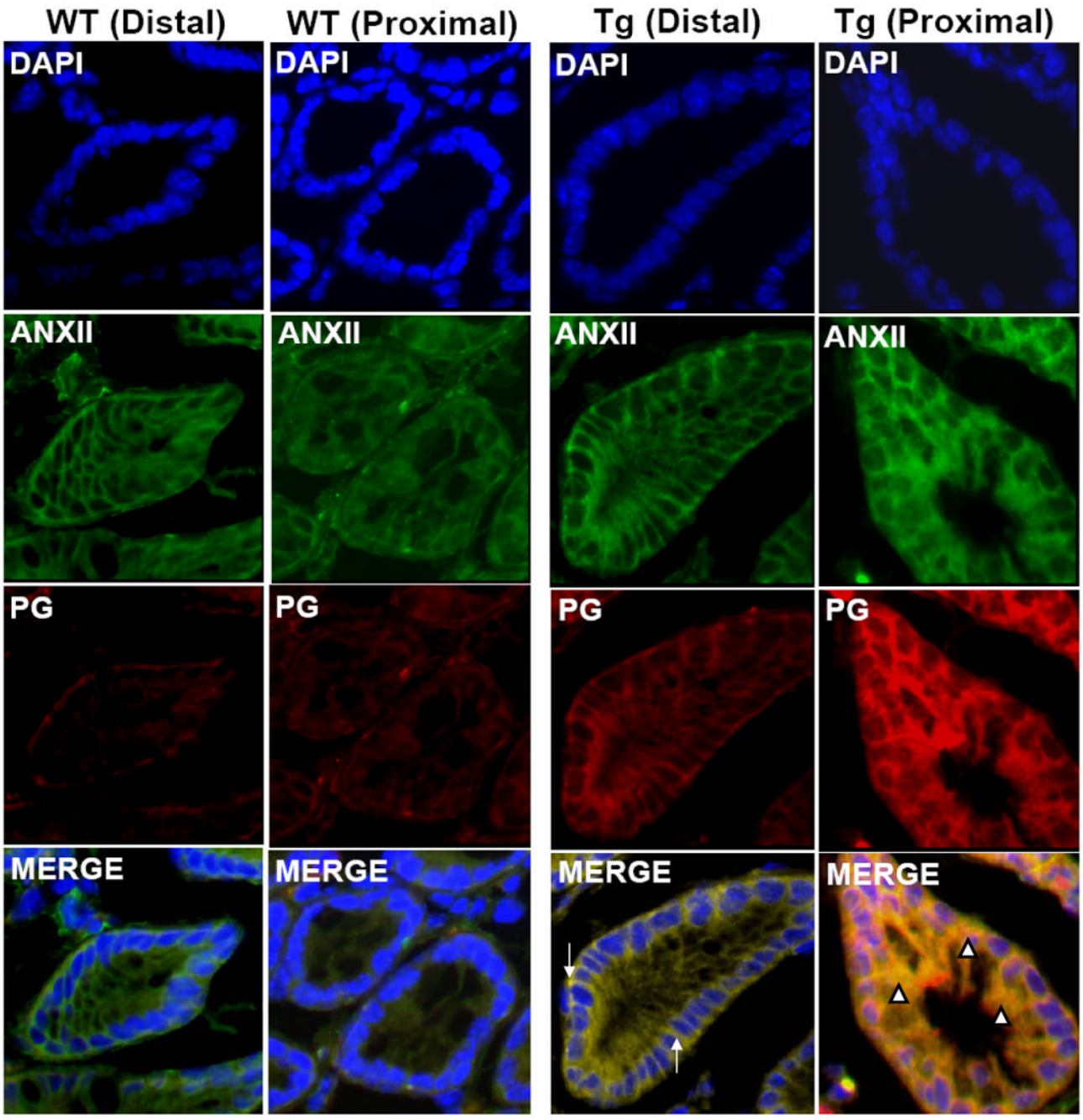

Figure 3. Immunolocalization of PG and ANX-II in distal and proximal colons

Frozen sections prepared from distal and proximal colons were stained with anti-PG-Abs and ANX-II-antibodies, which were detected by fluorescent microscopy using second antibodies tagged with either Texas Red (against PG-Abs) or FITC-green (against ANX-II-Abs). Representative sections from distal (**D**) and proximal (**P**) colons of WT mice and Fabp-PG (Tg) mice are shown (n = 3; 200×) ANX-II staining was localized predominantly in the apical-baso-lateral membranes of distal and proximal colons with minimal cytoplasmic staining in sections from WT mice. No staining for PG was detected in sections from WT mice. In the case of Fabp-PG (Tg) mice, in sections from distal colons, intense baso-lateral staining for ANX-II, which extended throughout the longitudinal crypts axis with minimal cytoplasmic

staining was observed. However, crypts from proximal colons of Tg mice exhibited dramatic increase in cytoplasmic staining for ANX-II with a gradient of increasing crypt base: surface immunoreactivity, along with perinuclear and nuclear staining. Equivalent levels of hgastrin gene were expressed in distal and proximal colons of Tg mice (as measured by quantitative Real Time PCR). However, relatively low levels of PG were retained in distal colonic crypts of Tg mice, while significant levels were retained within the proximal colonic crypts of Tg mice. Merged images of PG and ANX-II staining, demonstrated co-localization of PG and ANX-II only at the baso-lateral and apical membranes in the distal colonic crypts of Tg mice, with no co-localization intracellularly, which essentially resembled the pattern of ANX-II staining observed in the distal colons of Tg mice. In few mice, higher levels of PG were retained in the distal colonic crypts (representative data are presented in Supplementary Fig 1A). In spite of higher retention of PG in distal crypts of 10-20% of PG mice, PG, bound to ANX-II, remained co-localized at the apical and lateral membranes of the distal crypts (Supplementary Fig 1A). The merged images of proximal colonic crypts from Tg mice, on the other hand, demonstrated marked co-localization of PG and ANX-II staining at both the apical/lateral poles and within the cytoplasm and even nucleus (**Fig 3**). Arrows = co-localization of ANX-II and PG at plasma membranes; arrowheads = co-localization of ANX-II and PG intracellularly.

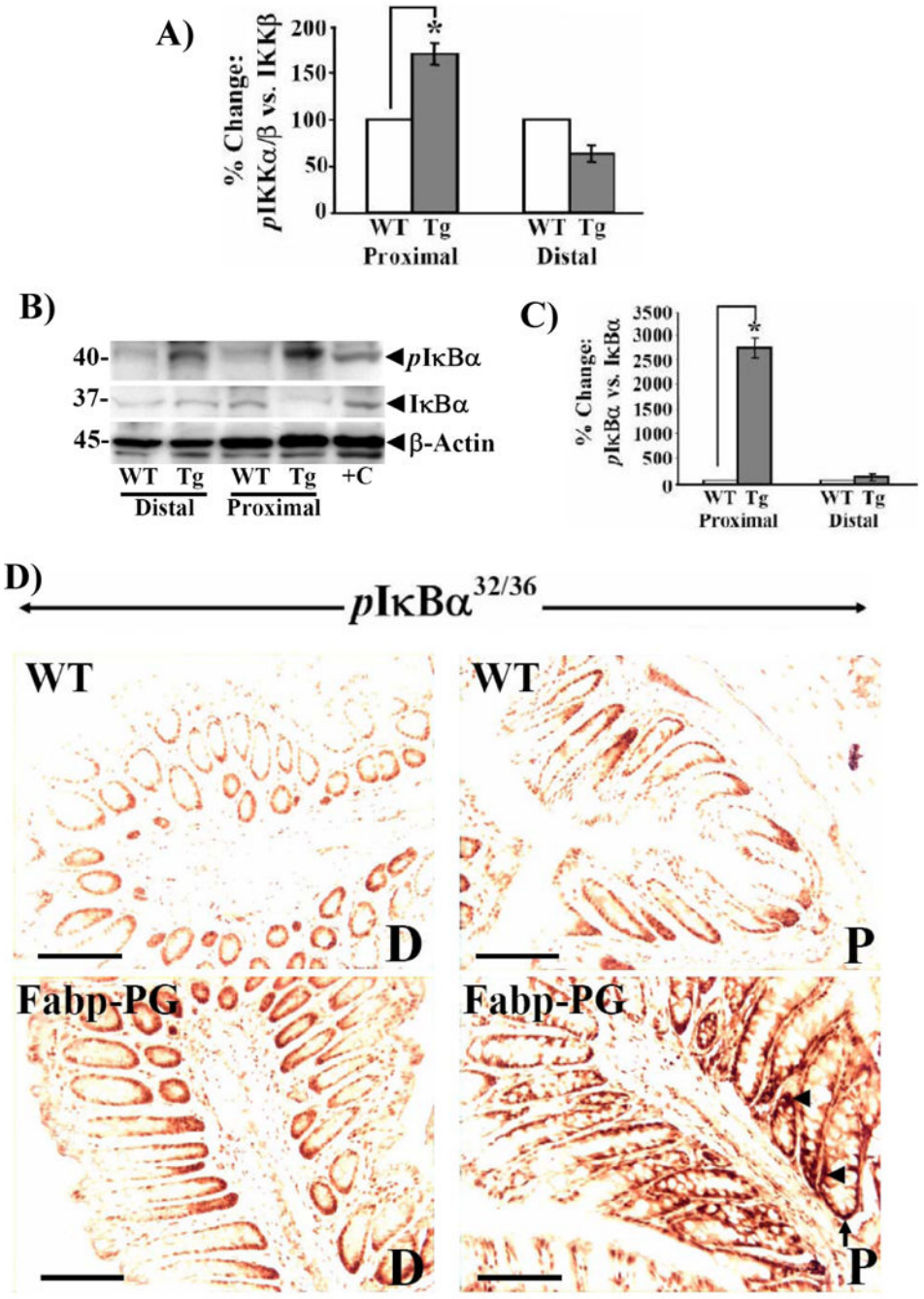

Figure 4. Phosphorylation of IKKα/β and IκBα in colons of Fabp-PG and WT mice

A. IKKα/β. Western blots of cellular extracts from isolated crypts were densitometrically analyzed, and ratio of phospho IKKα/β (*p*IKKα/β) to total IKK for WT samples were arbitrarily assigned a 100% value. % change in ratios for Fabp-PG vs. WT samples are shown as bar graphs. Data in each bar graph represents Mean ± SEM of 3 blots from 3 mice. * = $P<0.05$ versus WT values. **B. I**κ**B**α. Representative Western Blots for *p*IκBα and total IκBα in cellular extracts from proximal and distal colons of Fabp-PG and WT mice are shown; corresponding β-actin in the samples are presented as loading controls. +C = Hela cell extract used as positive control. In **C,** ratio of % changes in *p*IκBα versus total IκBα is shown as Mean ± SEM of 3 blots from 3 mice. **D. IHC of Ser$^{32/36}$-*p*I**κ**Bα** revealed significant accumulation in proximal

(P) but not distal (D) colons of Fabp-PG mice (**lower panel**) while the differences were less dramatic in proximal versus distal colonic crypts of WT mice (**upper panel**). (n = 3; bar = 50μm). Arrow heads = staining of *p*-IκBα in cytosol; Arrows = staining of phosphorylated IκBα in nuclei.

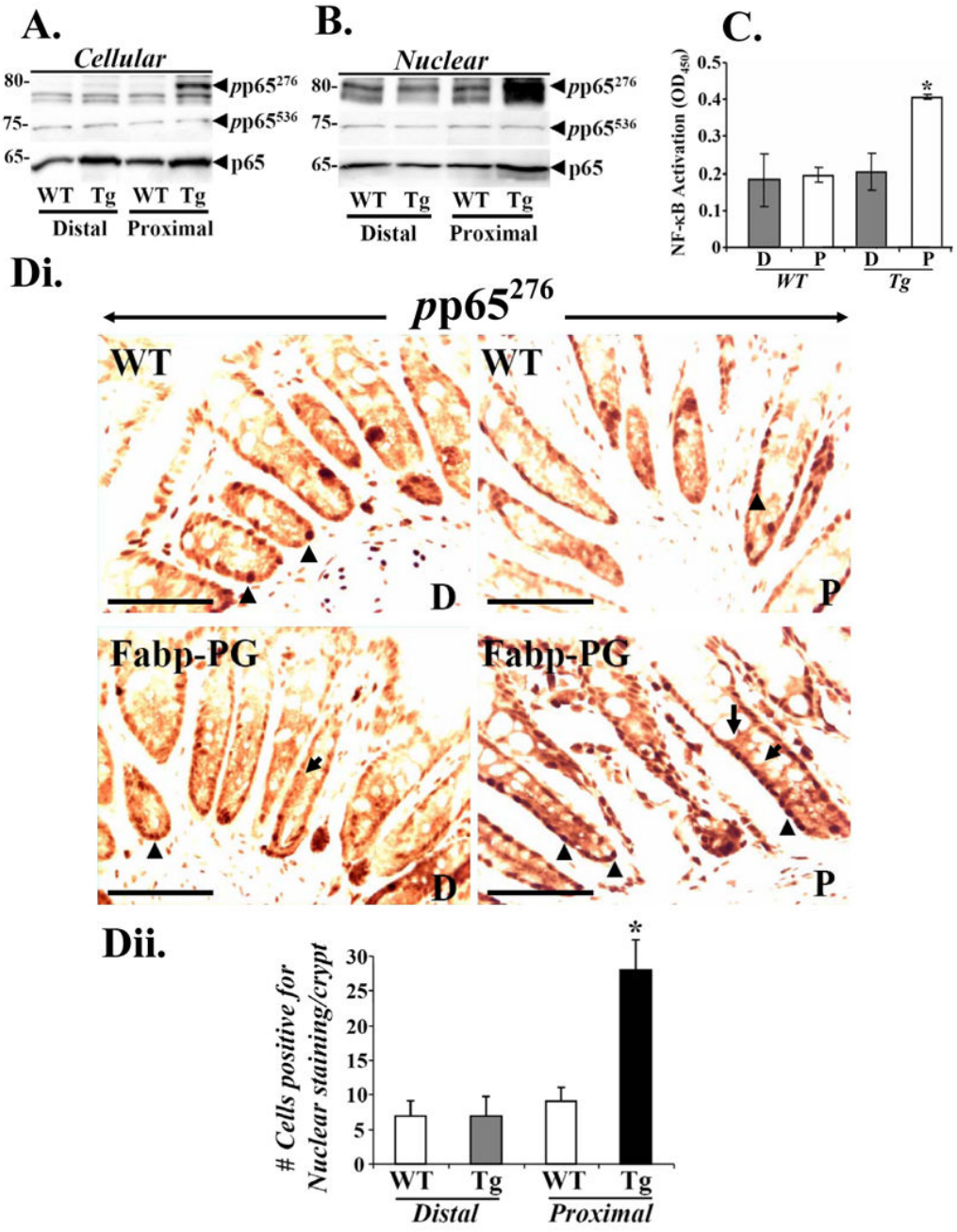

Figure 5. Phosphorylation and DNA binding of activated NF-κB p65

Representative Western Blots of cellular **(A)** and nuclear (**B**) extracts for *p*-p65^{276}, *p*-p65^{536} and total p65 are presented from distal and proximal crypts of wild type (**WT**) and Fabp-PG (**Tg**) mice. **C. DNA binding assay.** Relative levels of activated p65NF-κB in nuclear extracts of proximal and distal colons of WT and Tg mice, measured in a DNA binding assay using the TransAm™ p65 NF-κB Chemi Transcription Factor Assay Kit from Active Motif, are shown. Each bar graph represents mean ± SEM of three measurements from three mice. *=p<0.05 vs all other values. **Di. IHC of frozen sections with *p*-p65^{276} antibody.** Cytoplasmic and nuclear staining in proximal (P) and distal (D) colons of Fabp-PG mice (**lower panel**) and in distal and proximal colons from WT mice (**upper panel**) are shown. (n = 3; bar = 50μm). Arrowheads = phosphorylated p65-Ser^{276} in the nuclei of colonic crypts. Arrows= *p*-p65^{276} in cytosol of

crypts. **Dii**. Bar graph representing % cells/crypt positive for nuclear staining for *p*-p65^{276}. The data demonstrate several fold increase in % cells positive for phosphorylated p65 in nuclei of proximal colons of Tg mice compared to that in distal colons (n = 5).

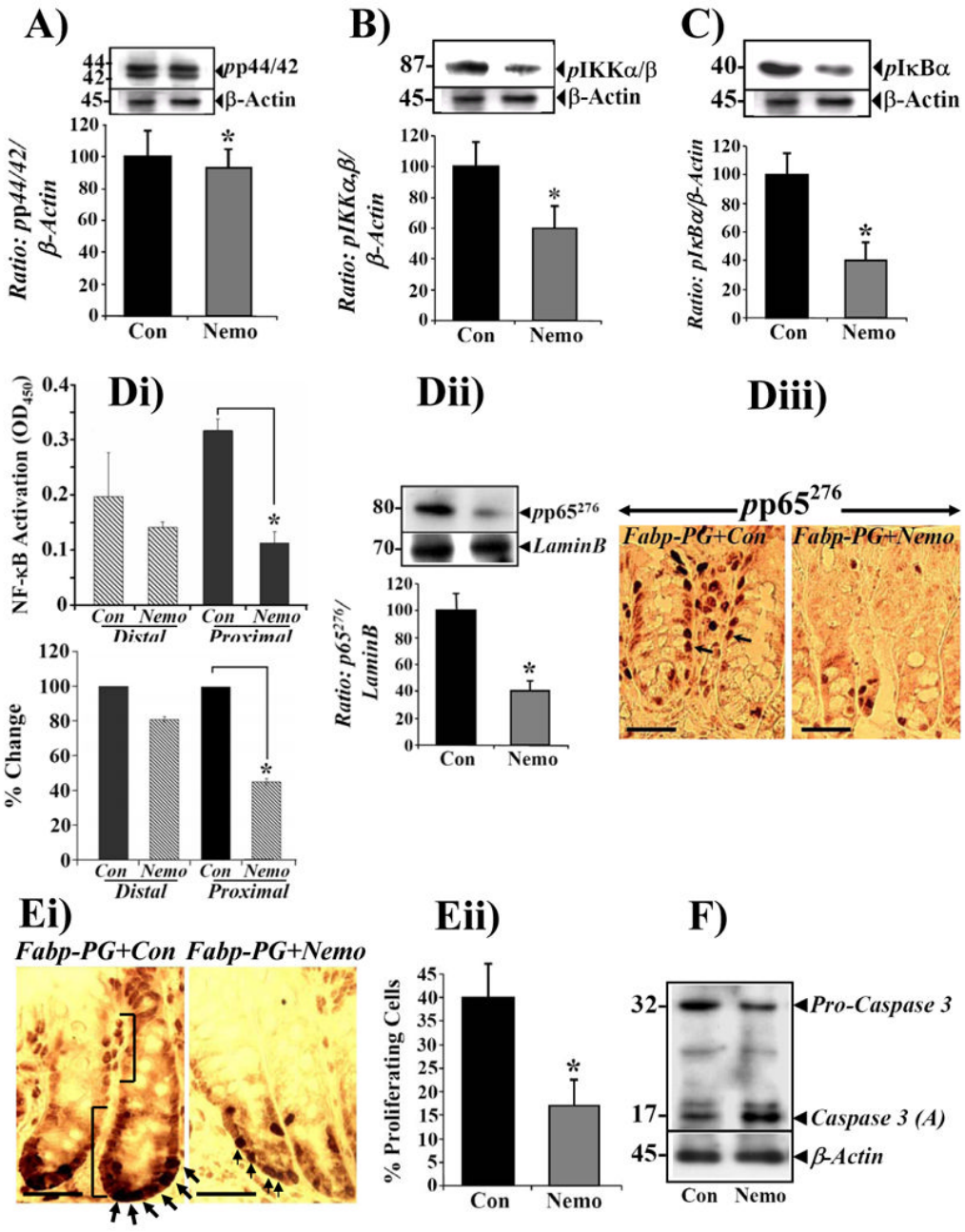

Figure 6. Effect of NEMO peptide on the levels of phosphorylated ERKs, IKKα/β, IκBα (A-C), p65NFκB (Di-iii), proliferation (Ei-ii) and apoptosis (F) in colonic crypts

Mice were divided into two groups and injected, once a day for four days with either NEMO or control peptide (as described in Methods). Two hours after last injection, colonic crypts were isolated and fractionated into cellular and nuclear extracts. Data obtained from proximal colonic crypts of Fabp-PG mice are presented. **A-C:** Representative Western blots from NEMO versus control peptide treated samples are shown from one of four mice/group. The data in the Western blots of the cellular extracts were densitometrically analyzed from all mouse samples, and the ratios of: phospho ERK1/2 (*p*p44/42; **A**), phospho IKKα/β (*p*-IKKα/β); **B**) and phospho IκBα (*p*-IκBα); **C**) to β-actin, were arbitrarily assigned a 100% value. % change in ratios for NEMO peptide versus control peptide values are shown as bar graphs. Data in each bar graph

represents Mean ± SEM of 4 blots from 4 mice. **Di. DNA binding assay.** NEMO peptide significantly inhibited NFκB activation, measured in a DNA binding assay with nuclear extracts from proximal, but not distal, colonic crypts of Fabp-PG mice, compared to levels measured in control peptide samples (upper panel, **Di**); % change in the relative levels of activated NFκB in control peptide vs NEMO peptide treated samples are shown in lower panel of **Di**. Each bar represents mean ± SEM values from 3 measurements from 3 separate mice. *=p<0.05 vs corresponding control values. **Dii. Phosphorylation status of p65.** Representative Western blots of nuclear extracts were densitometrically analyzed, and the ratio of *p*-p65^{276} to LaminB, was arbitrarily assigned a 100% value. % change in ratios for NEMO peptide versus control peptide treated values are shown as bar graphs. For data in **A-D**, *=P<0.05 versus control peptide values. D**iii. IHC of frozen sections with anti- *p*-p65^{276} antibody.** Cytoplasmic and nuclear staining (**arrows**) in proximal colons of Fabp-PG mice, receiving either control peptide (**left panel**) or treated with NEMO (**right panel**), are shown (n = 3; bar = 50μm). Note significant reduction in staining for *p*-p65^{276} in sections prepared from proximal colon of NEMO-treated animals. **E. Effect of NEMO peptide on PI of colonic crypts. Ei.** Representative sections from Fabp-PG mice treated with either control peptide (**left panel**) or NEMO (**right panel**) were stained with BrdU antibody. Similar to **Diii**, NEMO peptide significantly reduced BrdU incorporation into S-phase cells, to basal levels. Arrows point to BrdU staining of nuclei. **Eii.** PI was calculated from 40 crypts/group of 4 mice each, based on number of positive cells along the longitudinal crypt axis. PI decreased significantly in NEMO-treated colonic crypts. Each bar = mean ± SEM of 40 crypts. *=p<0.05 vs control values **F. Effect of NEMO peptide on Caspase 3 activation.** Representative Western blot of cellular extracts from one of four mice/group is presented. Treatment of Fabp-PG mice with NEMO peptide resulted in a significant increase in the relative levels of activated (A) caspase 3, with a concomitant decrease in relative levels of pro-caspase 3, in proximal colonic crypts when compared to that in mice treated with the control peptide. β-actin was used as loading control. The relative levels of phosphorylated kinases, PI and activated caspase 3 in distal crypts of Fabp-PG mice was not significantly altered in NEMO versus control treated mice (data not shown), since these levels were not changed significantly in response to PG as presented in Figs 1, 2, 4, and 5. Similarly, the relative levels of phosphorylation of the indicated kinases, PI and activated caspase 3 were not altered significantly in NEMO versus control peptide treated WT mice (data not shown), suggesting that IKKα/β/NFκB pathway does not play a significant role in the basal growth of colonic crypts in the WT mice as suggested by data presented in Figs 1, 2, 4, and 5.